



REGULAR PAPER

Haotian Hang · Bin Yu · Yang Xiang · Bin Zhang · Hong Liu

# An objective-adaptive refinement criterion based on modified ridge extraction method for finite-time Lyapunov exponent (FTLE) calculation

Received: 26 March 2018 / Revised: 9 May 2019 / Accepted: 15 July 2019 / Published online: 8 October 2019  
© The Visualization Society of Japan 2019

**Abstract** Visualizing finite-time Lyapunov exponent (FTLE) efficiently and accurately has long been a research objective in identifying the coherent structures of turbulence or vortex flows. In this field, adaptive mesh refinement shows its effectiveness. The proposed objective-adaptive refinement (OAR) criterion can refine adaptive particles in the vicinity of FTLE ridges by a modified gradient climbing method. While error-based refinement methods suffer from ineffective refinement when the initial velocity field contains error, and refinement methods based on FTLE magnitude have issues with undulate ridges, our objective OAR criterion always steers the refinement toward the vicinity of FTLE ridges. Testing cases include Bickley jet, mild FTLE ridge and experimental single vortex, three-dimensional ABC flow. The results demonstrate that the proposed OAR criterion can give the right refinement region, and thus enhance computation efficiency, by means of accurate extraction of FTLE ridges.

**Keywords** Flow structures visualization · Objective-adaptive refinement (OAR) · Lagrangian coherent structures (LCS) · Finite-time Lyapunov exponent (FTLE)

## 1 Introduction

Visualization of the flow field has always been one of the hot topics in the study of fluid dynamics. Details of complex unsteady flows, such as turbulent flow, vortices and shear layer, are difficult to demonstrate if one only considers its velocity field or vorticity field. Thus, using post-process methods is important to more clearly visualize the flow field (Haller 2015; Zhang et al. 2017). Researchers have proposed numerous flow structure extraction methods based on Eulerian and Lagrangian considerations for the computational visualization of a flow field. The methods based on Eulerian consideration such as Q-criterion (Hunt 1988),  $\Delta$ -criterion (Chong et al. 1990),  $\lambda_2$ -criterion (Jeong and Hussain 1995), Rotex method (Tian et al. 2018) can give a good visualization of transient flow phenomena. In 2000, Haller and Yuan (2000) systematically studied Lagrangian coherent structures (LCSs) to describe the most attracting, repelling and shearing material lines in a flow field. Since then, LCSs have been widely applied in the visualization of complex flow fields (Tang et al. 2010; Shadden et al. 2007; Beron Vera et al. 2015; Karch et al. 2016; Tallapragada et al. 2011; Liang et al. 2019).

In order to find material interface in flow field, Haller (2001) demonstrated that the extremum of finite-time Lyapunov exponent (FTLE) can be regarded as LCS ridge. Finding these surfaces from experimental or numerical results can give an easy and useful way to understand the material transport and mixture in the flow field (Haller 2015). Particular flow fields such as experimental data or turbulence flows are in high

H. Hang · B. Yu · Y. Xiang · B. Zhang (✉) · H. Liu  
School of Aeronautics and Astronautics, Shanghai Jiao Tong University, Shanghai, China  
E-mail: zhangbin1983@sjtu.edu.cn  
Tel.: +8613817855406

noise level, which increases the difficulties in visualizing LCS. Mathur et al. (2007) proposed a gradient climbing method and it accurately locates the FTLE ridges as LCS. To define the ridge more clearly, elliptic LCSs (Blazevski and Haller 2014), parabolic LCSs (Froyland and Padberg-Gehle 2014) and hyperbolic LCSs (Duc and Siegmund 2008) are given. Parabolic LCSs are unsteady zonal jet cores in the flow field (Hadjighasem and Haller 2014), and the evolving parabolic LCS can act as a transport barrier which can prevent the mixing across the coherent structure. Elliptical LCSs are the Lagrangian vortex boundaries, which can identify the boundary of vortex rings (Karrasch et al. 2015). Hyperbolic LCSs are repelling and attracting LCSs, which can converge an area to a single line. In most cases, hyperbolic LCSs coincide with the FTLE ridges, but they are not the same (Haller 2011), in some particular cases in real life. Although these calculations are mainly based on the eigenvector of the Cauchy-Green tensor, FTLE (the eigenvalue of the Cauchy-Green tensor) can also express the characteristic of the tensor. Thus, developing new methods to promote the efficiency and accuracy of FTLE ridge visualization is still important (Green et al. 2007).

Adaptive mesh refinement (AMR) is a method for adapting the accuracy of a solution within certain sensitive or turbulent regions of simulation (Plewa et al. 2005; Huang and Russell 2011). This technique has been widely applied in CFD and proved to reduce the cost of calculation (Barakat and Tricoche 2013; Wang et al. 2016; Ng and Wong 2007; Jimbo and Tanahashi 2003; Keith and Demetri 1991; Berger and Colella 1989). AMR has also been used in FTLE computation, which can improve the efficiency of calculation by a large amount. Garth et al. (2007) first developed the method of AMR in LCS. Miron et al. (2012) applied AMR in FTLE calculation in anisotropic mesh using a commercial software. Based on this, Fortin et al. (2015) compared various kinds of adaptive methods to provide a more accurate method. The refinement criterion of all these methods is based on the error of FTLE field.

However, AMR in LCS methods based on error may be unable to find FTLE ridge accurately in the cases mentioned in Sect. 4.3. For this reason, an adaptive refinement method based on the extraction of FTLE ridge should be proposed. Sadlo and Peikert (2007) applied the method based on the magnitude of FTLE (Lipinski and Mohseni 2010) into the adaptive refinement of FTLE calculation. However, FTLE ridge is not definitely the maximum of FTLE value, especially when the FTLE field is undulating because of the error in initial data. A better ridge extraction method provided in Mathur et al. (2007) is intended to find FTLE ridge in chaotic flow field by a gradient climbing method. Nevertheless, it was unable to find FTLE ridge when the FTLE ridge is relatively mild as illustrated in Sect. 4.2. In this study, an objective-adaptive refinement (OAR) criterion based on a modified gradient climbing method is proposed. This criterion can give right refinement region, and thus enhance computation efficiency, by means of accurate extraction of FTLE ridges.

The rest of the paper is organized as follows. In Sect. 2, the principle and definition of LCS is introduced. In Sect. 3, the OAR method is described and applied in FTLE calculation. Two 2D analytical examples, one experimental example and one 3D analytical case are demonstrated in Sect. 4. The result and visualization obtained by different methods are also compared. The conclusions are presented in Sect. 5.

## 2 Finite-time Lyapunov exponent (FTLE) description

### 2.1 The definition of FTLE

Transport in dynamical system is often studied by the trajectory of spatial particles. Lyapunov exponent can be used in the moving trajectory of spatial particles. Finite-time Lyapunov exponent (FTLE)  $\sigma_t^T(\mathbf{x})$ , is a scalar quantity. When used in the computation of fluid, FTLE expresses the average separation degree for a fluid particle and the trajectory of its surrounding fluid particles from  $t$  to  $t + T$ . The computational formula of  $\sigma_t^T(\mathbf{x})$  is as follows:

$$\sigma_t^T(\mathbf{x}) = \frac{1}{|T|} \ln \sqrt{\lambda_{\max}(\mathcal{A})}, \quad (1)$$

where  $\mathcal{A}$  is a symmetrical matrix, and the result of the moving trail spatial derivative matrix multiplies its transposition.  $\lambda_{\max}(\mathcal{A})$  is its maximum eigenvalue of  $\mathcal{A}$ . The moving trail of the fluid particle from  $t$  to  $t + T$ , is marked as  $\phi_t^{t+T}(\mathbf{x})$ . Then, the symmetrical matrix  $\mathcal{A}$  is as follows:

$$\mathcal{A} = \left[ \frac{d\phi_t^{t+T}(\mathbf{x})}{d\mathbf{x}} \right]^* \frac{d\phi_t^{t+T}(\mathbf{x})}{d\mathbf{x}} \quad (2)$$

where  $\frac{d\phi_t^{t+T}(\mathbf{x})}{d\mathbf{x}}$  denotes the Jacobian of  $\phi_t^{t+T}(\mathbf{x})$ , and  $*$  refers to matrix transposition.

## 2.2 Literature review of fast FTLE calculation

### 2.2.1 Adaptive mesh refinement (AMR) based on error used in FTLE calculation

There are various studies focusing on the adaptive mesh refinement used in FTLE calculation (Lipinski and Mohseni 2010; Miron et al. 2012; Garth et al. 2007). Though the definition of error is different, the inherent property is the same. In this paper, we compared the proposed method with the method described in Garth et al. (2007), which is showed as Eq. (3).

$$\begin{aligned}\varepsilon_{i,j} &= \|Sf_{i,j} - f_{i,j}\| \\ Sf_{i,j} &= \frac{1}{32}(9f_{i+1,j} + 9f_{i-1,j} + 9f_{i,j+1} + 9f_{i,j-1} \\ &\quad - f_{i+2,j} - f_{i-2,j} - f_{i,j+2} - f_{i,j-2})\end{aligned}\quad (3)$$

### 2.2.2 Ridge extraction method

Extracting FTLE ridge has long been a research hot point (Mathur et al. 2007; Lipinski and Mohseni 2010). Sadlo and Peikert (2007) first applied this method in the adaptive refinement of FTLE calculation, and used the magnitude of FTLE as criterion of refinement as in Eq. (4).

$$\sigma_t^T(\mathbf{x})_{\text{local}} \geq \alpha \sigma_t^T(\mathbf{x})_{\text{max}} \quad (4)$$

This method may give incorrect refinement region when there is noise in the origin data. Mathur et al. (2007) provides us a new method to find accurate ridge in noisy data. The process is as follows. Firstly, the mesh nodes were chosen using Eq. (5).

$$|\nabla \sigma_t^T(\mathbf{x})|_{\text{local}} \geq \alpha |\nabla \sigma_t^T(\mathbf{x})|_{\text{max}} \quad (5)$$

Then, the particles are moved through vector  $\nabla \sigma_t^T(\mathbf{x})$ . The cease conditions are shown in Eqs. (6) and (7).

$$\min\{\lambda_{1,2}(\nabla^2 \sigma_t^T(\mathbf{x}))\} < 0 \quad (6)$$

$$\theta \left\langle e_t^T(\mathbf{x})_{\nabla^2 \sigma_t^T(\mathbf{x})}, \nabla \sigma_t^T(\mathbf{x}) \right\rangle \leq \theta_{\min} \quad (7)$$

However, these methods have problems and fail to refine right region in cases, such as in Sects. 4.2 and 4.3. Our method introduced in Sect. 3 is based on this method, but the cease condition has been revised.

## 2.3 Error definition

In this paper, the error used to compare different methods in Sect. 4 is defined as Eq. (8).

$$\begin{aligned}\varepsilon &= \frac{\sum_{i=1}^{N_{\text{particles}}} \varepsilon_i}{N_{\text{particles}}} \\ \varepsilon_i &= \|Sf_i - f_i\|,\end{aligned}\quad (8)$$

where  $Sf_i$  is the interpolation of  $f_i$  by the surrounding particles in a very dense mesh.

## 3 Proposed OAR based on modified ridge extraction method

Non-adaptive LCS calculation consumes considerable computational resources. If more resources are allocated to the vicinity of LCS ridges and less attention is paid on relatively smooth regions, adaptive methods will save significant computational resources. The proposed whole algorithm is shown as Algorithm 1 in Sect. 3.1.

Several AMR methods in LCS use the traditional AMR method, which focuses on error (Fortin et al. 2015; Garth et al. 2007) or the magnitude of FTLE (Lipinski and Mohseni 2010; Sadlo and Peikert 2007). In

this article, the proposed OAR criterion allocates refinement particles at the vicinity of LCS, which is discussed in Sect. 3.2.

### 3.1 Proposed whole algorithm

In this paper, our method includes two layers of refinement particles, which can be illustrated as Algorithm 1. From line 2 to line 4 in Algorithm 1, the level-1 particles are dispersed as a cartesian coordinate in a form of one-dimensional index, and FTLE of them are calculated just like the traditional LCS method. After the calculation, the level-2 particles are dispersed as mentioned in Sect. 3.2. The index of the level-2 particles is linked with the level-1 particles. From line 5 to line 11, the particles are chosen based on an appropriate  $\alpha$ , and then the FTLE field of the level-2 particles are calculated by the APs through particle motion and FTLE calculation. Then, all the results are put into a new mesh for the next step calculation. The dispersion and calculation of level-3 particles is similar to that the one of the level-2 particles except for the refinement rule is based on FTLE as shown from line 12 to line 16 in Algorithm 1.

---

**Algorithm 1** Proposed OAR for LCS

---

```

1: read data                                ▷ the first layer
2: initialize the level-1 particles
3: advect level-1 particles to endtime
4: calculate FTLE of each particle           ▷ the second layer
5: find the appropriate  $\alpha$ 
6: find the level-1 particles which need refinement
7: displace the level-2 particles
8: link the index of the level-2 particles with the index of the level-1 particles
9: advect level-2 particles to endtime
10: calculate FTLE of each particle
11: put the result into a new mesh using index linking      ▷ the third layer
12: find the level-2 particles which need refinement
13: displace level-3 particles
14: link the index of the level-3 particles with the index of the level-2 particles
15: advect level-3 particles to endtime
16: calculate FTLE of each particle
17: put the result into a new mesh using index linking
18: output

```

---

### 3.2 The proposed refinement criterion based on modified ridge extraction method

Precious studies (Garth et al. 2007; Miron et al. 2012; Sadlo and Peikert 2007) showed that the criterion of where to refine the mesh of existing research remains that of traditional methods, which is according to error. This is defined in Eq. (8). This has been proved to be efficient in most cases such as Garth et al. (2007), Miron et al. (2012), Sadlo and Peikert (2007) and Sect. 4.1. However, as in some cases, these methods may be not suitable, for the refinement particles which may not be the right position.

In this article, refinement particles are placed near the FTLE ridge. Firstly,  $\sigma_t^T(\mathbf{x})$  is calculated in a coarse mesh. And then, like the method provided in Mathur et al. (2007), the particles for which  $|\nabla \sigma_t^T(\mathbf{x})|$  is bigger than a given threshold, and they move in the  $\nabla \sigma_t^T(\mathbf{x})$  field. In this paper, we define the threshold as in Eq. (9).

$$|\nabla \sigma_t^T(\mathbf{x})|_{\text{local}} \geq \alpha |\nabla \sigma_t^T(\mathbf{x})|_{\text{max}} \quad (9)$$

These particles would move until  $\nabla \sigma_t^T(\mathbf{x})$  becomes so small that the particles would hardly move, which means the local FTLE ridge is obtained.

When the motion of the particles is ceased, the four particles of the coarse mesh surrounding the final position are the particles which needed to be refined. When some of the particles are moving across the boundary of computational domain, the particles are seen as invalid. The particles which are chosen firstly

1. particles which satisfy  $|\nabla \sigma_i^T(x)|_{local} \geq \alpha |\nabla \sigma_i^T(x)|_{max}$  are chosen, namely the white region in the picture
2. particles move in  $\nabla \sigma_i^T(x)$  field
3. particles for which  $|\nabla \sigma_i^T(x)|$  is too small are particles need refinement

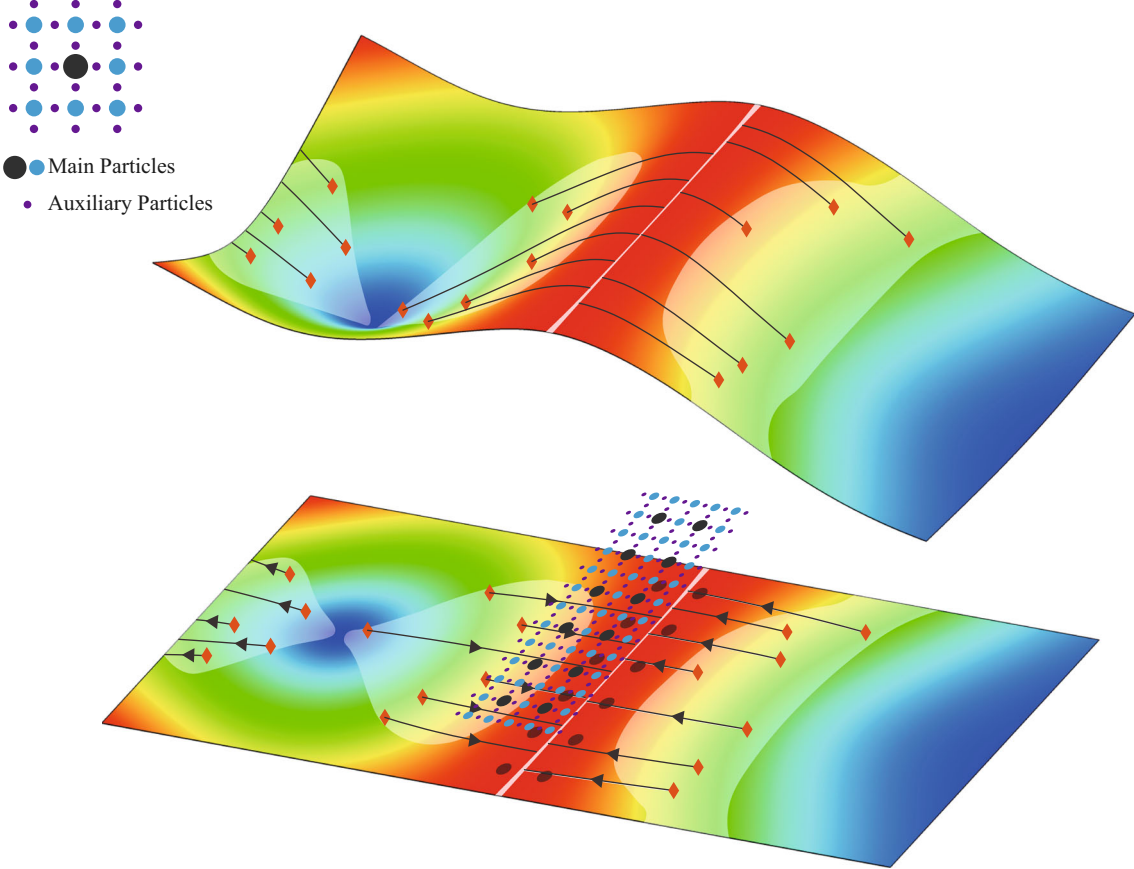


**Fig. 1** Illustration of the objective-adaptive refinement (OAR) method

are not necessarily the particles need refinement, and the phenomenon is illustrated in Fig. 1. The firstly chosen particles are labeled as red.

For each particle which is needed for refinement, nine main particles (shorten for MPs) and 24 auxiliary particles (shorten for APs) are placed as illustrated in the right top part of Fig. 1. The MPs, namely the blue particles in Fig. 1, are needed to calculate FTLE, in which the dark blue particles are the particles needed to refine the lower layer. The APs, namely the purple particles, are particles which assist in the FTLE calculation.

### 3.2.1 The limiting threshold $\alpha$ in OAR method

It is a problem in choosing the parameter  $\alpha$  mentioned in Eq. (9). The value of  $\alpha$  does not effect to the amount of the refinement particles if it is small enough, because the particles would converge to LCS ridge through the motion, which is illustrated Fig. 2. We can find that compared with other criterion, the proposed refinement criterion is superior because the refinement region would not be too large to be useful when the parameter changes as showed in Fig. 2.

For this reason, the method of finding an appropriate  $\alpha$  in our algorithm is as follows. Firstly, a relatively large  $\alpha$  is given, and the total number of refinement particles is counted. Then,  $\alpha$  decreases by a small step  $\Delta\alpha$ , which is chosen to be 0.05 in this article, and the amount of the refinement particles corresponding to the new  $\alpha$  is compared with the former one. If the difference is relatively small, the  $\alpha$  is the one we need. Because the refinement process includes particle motion, the calculation amount is relatively big. To reduce

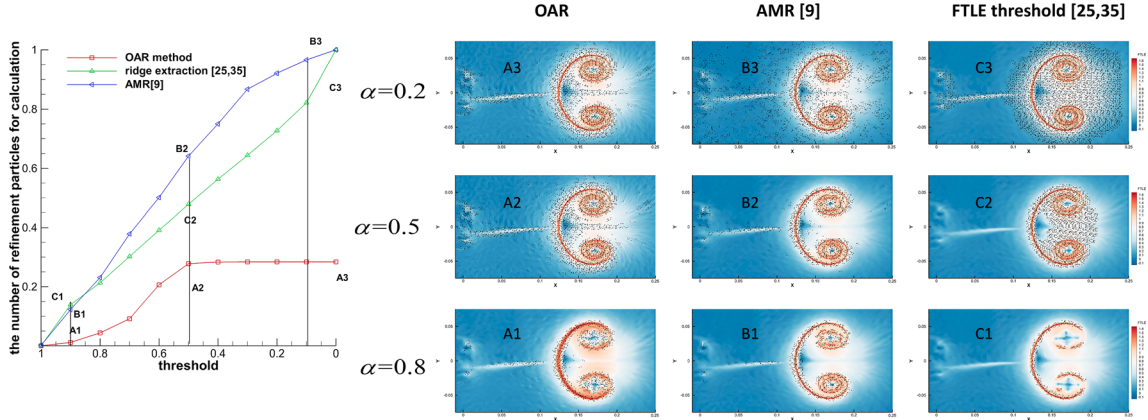


**Fig. 2** Illustration of the influence of parameter change for different criteria

the calculation burden, for each  $\alpha$ , only the particles which have not moved move. For the proposed method, if  $\alpha$  is chosen to be too large, and thus few particles are chosen in the first step, some FTLE ridges would not be refined. On the other hand, when  $\alpha$  is chosen to be small enough, the refinement region would not change.

#### 4 Results comparison

The proposed method is compared with AMR methods which is based on error (Garth et al. 2007), a ridge extraction method based on the magnitude of FTLE (Sadlo and Peikert 2007; Lipinski and Mohseni 2010), and a ridge extraction method based on gradient ascending method (Mathur et al. 2007). Through the comparison, the proposed OAR method is proved to be superior to other methods in finding the correct refinement regions which are near the FTLE ridges.

For the comparison of different methods, parameter  $\alpha$  in methods other than the proposed OAR method is not the same. Instead, parameter is chosen in order to ensure that the proportion of refinement particles is nearly the same as in the proposed OAR method.

##### 4.1 Bickley jet

The Bickley jet is an ideal model of geophysical flows (Onu et al. 2014). This model is a jet like flow with counter rotating vortices, and can be an approximation of the Gulf Stream and the polar night jet perturbed by a Rossby wave. The velocity field can be given as follows:

$$\mathbf{v}(x, y, t) = (-\partial_y \psi, \partial_x \psi) \quad (10)$$

$$\psi(x, y, t) = \psi_0(x, y) + \psi_1(x, y, t) \quad (11)$$

$$\psi_0(x, y) = c_3 y - UL_y \tanh \frac{y}{L_y} + \varepsilon_3 UL_y \operatorname{sech}^2 \frac{y}{L_y} \cos k_3 x \quad (12)$$

$$\psi_1(x, y, t) = UL_y \operatorname{sech}^2 \frac{y}{L_y} \Re \left[ \sum_{n=1}^2 \varepsilon_n f_n(t) e^{ik_n x} \right] \quad (13)$$

As a forcing function, a solution running on the chaotic attractor of the damped and forced Duffing oscillator is chosen, as follows:

$$\frac{d\phi_1}{dt} = \phi_2 \quad (14)$$

$$\frac{d\phi_2}{dt} = -0.1\phi_2 - \phi_1^3 + 11 \cos(t) \quad (15)$$

$$f_{1,2}(t) = 2.625 \times 10^{-2} \phi_1(t/6.238 \times 10^5) \quad (16)$$

The parameter values are:  $U = 62.66$ ,  $c_2 = 0.205U$ ,  $c_3 = 0.461U$ ,  $L_y = 1.77 \times 10^6$ ,  $\varepsilon_1 = 0.0075$ ,  $\varepsilon_2 = 0.04$ ,  $\varepsilon_3 = 0.3$ ,  $L_x = 6.371 \times 10^6\pi$ ,  $k_n = 2n\pi/L_x$ ,  $\sigma_1 = 0.5k_2(c_2 - c_3)$ ,  $\sigma_2 = 2\sigma_1$ . The integration time is  $T = 4L_x/U$ , and the domain is  $x \in [0, 2 \times 10^7]$ ,  $y \in [-4 \times 10^6, 4 \times 10^6]$ .

Putting the results of different refinement criteria together in Fig. 3, it can be found that the refinement regions are all near the FTLE ridge with little difference. Because of this, all these methods can reduce error efficiently, which can be illustrated in Fig. 4.

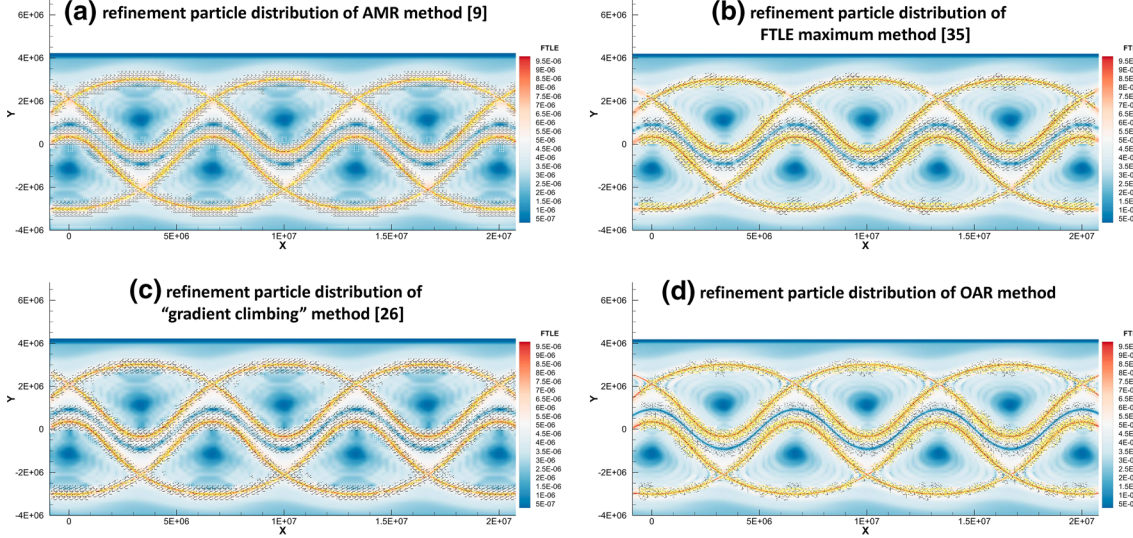


**Fig. 3** Bickley jet model. FTLE field and refinement particle distribution using an initial mesh of  $125 \times 50$  by **a** AMR method (Garth et al. 2007) (total particle number is 450,859); **b** the proposed OAR method (total particle number is 425,119); **c** ridge extraction method based on the magnitude of FTLE (Sadlo and Peikert 2007; Lipinski and Mohseni 2010) (total particle number is 601,933); **d** ridge extraction method based on gradient ascending method (Mathur et al. 2007) (total particle number is 442,081)

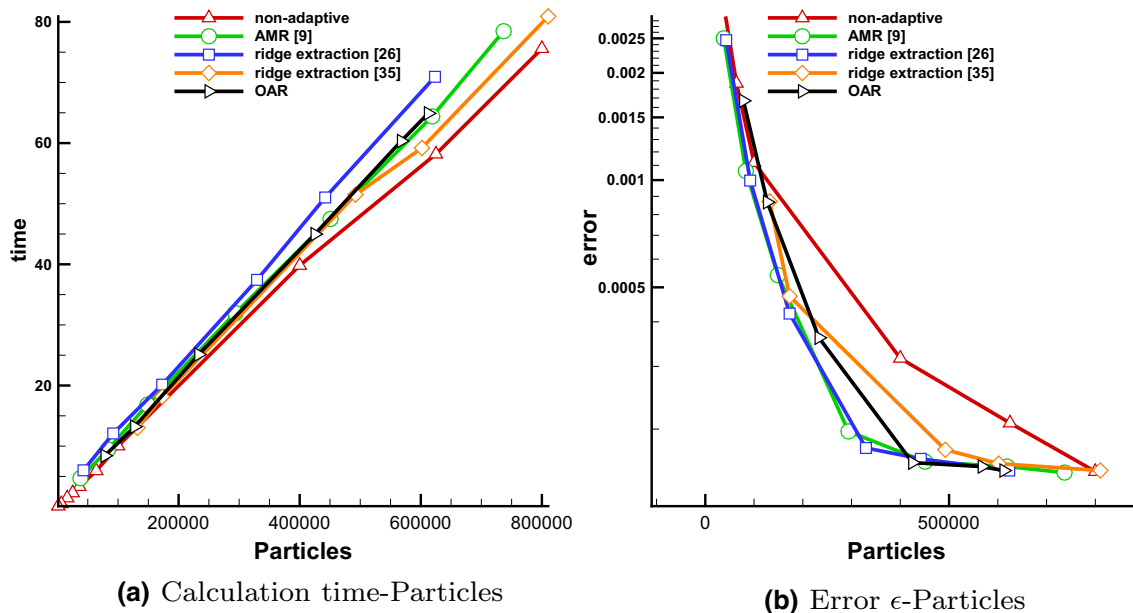


**Fig. 4** Comparison of the calculation time and errors of the non-adaptive and different adaptive criteria

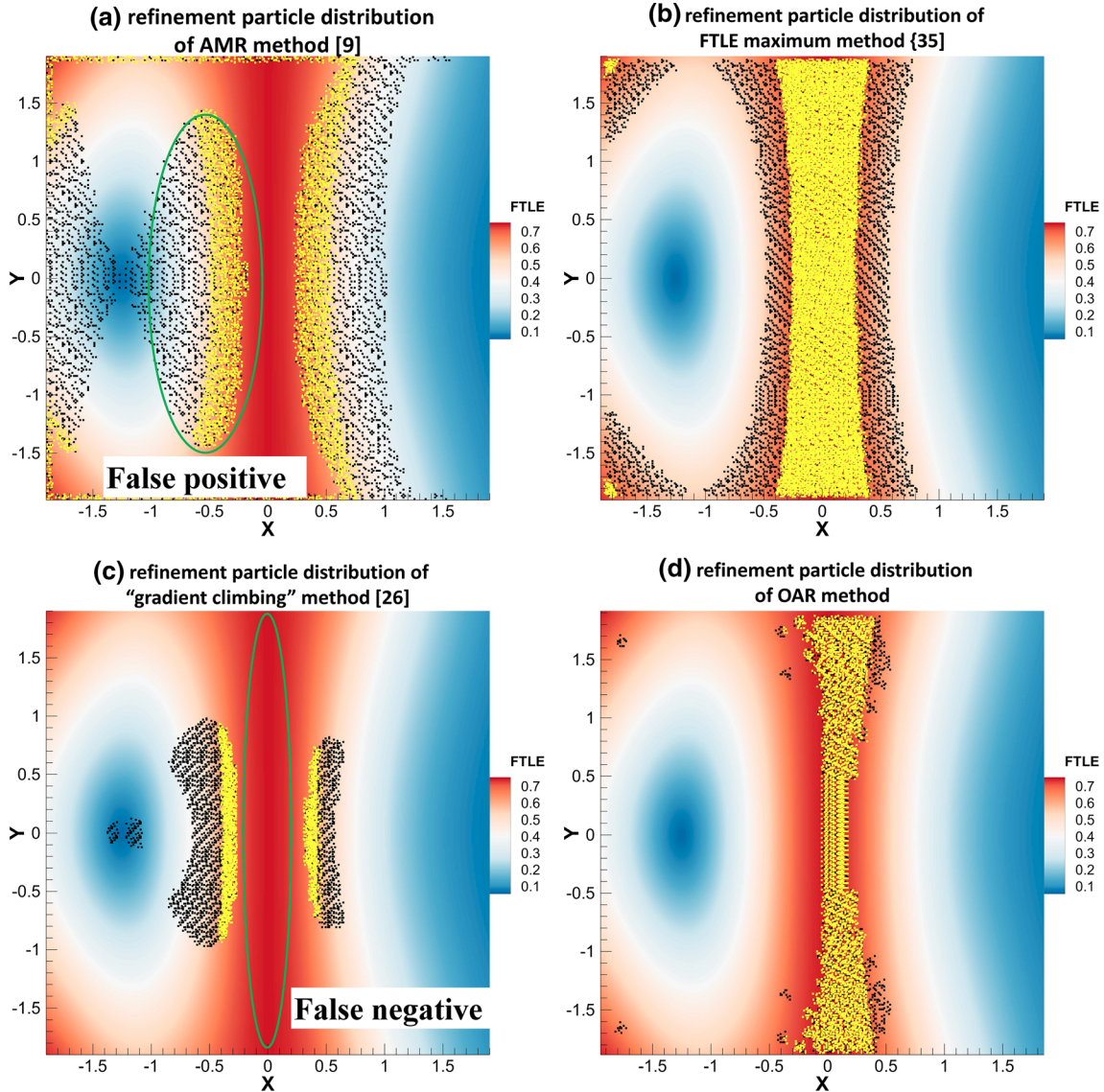


**Fig. 5** FTLE field and refinement particle distribution using an initial mesh of  $100 \times 100$  by **a** AMR method (Garth et al. 2007) (total particle number is 288,784); **b** the proposed OAR method (total particle number is 233,410); **c** ridge extraction method based on the magnitude of FTLE (Sadlo and Peikert 2007; Lipinski and Mohseni 2010) (total particle number is 398,860); **d** ridge extraction method based on gradient ascending method (Mathur et al. 2007) (total particle number is 281,887)

#### 4.2 A case with mild FTLE ridge

The flow field has an interesting feature which is that there occurs an FTLE ridge at  $x = 0$ , and the ridge is mild, which has been illustrated in Haller (2011). The speed field is as follows

$$\begin{aligned}\dot{x} &= 1 + \tanh^2 x \\ \dot{y} &= -\frac{2 \tanh x}{\cosh^2 x} y\end{aligned}\tag{17}$$

For most cases, FTLE ridge is sharp, such as the case in Sects. 4.1 and 4.3. However, in this case, the FTLE ridge is relatively mild, for this reason, simply applying the method in Mathur et al. (2007) into adaptive refinement method would give false positive results and not refine the surrounding of FTLE ridge.

The refinement particles dispersion is shown in Fig. 5. From the comparison of the four subfigures, it is shown that in Fig. 5a, c, both methods fail to refine the regions around the FTLE ridge.

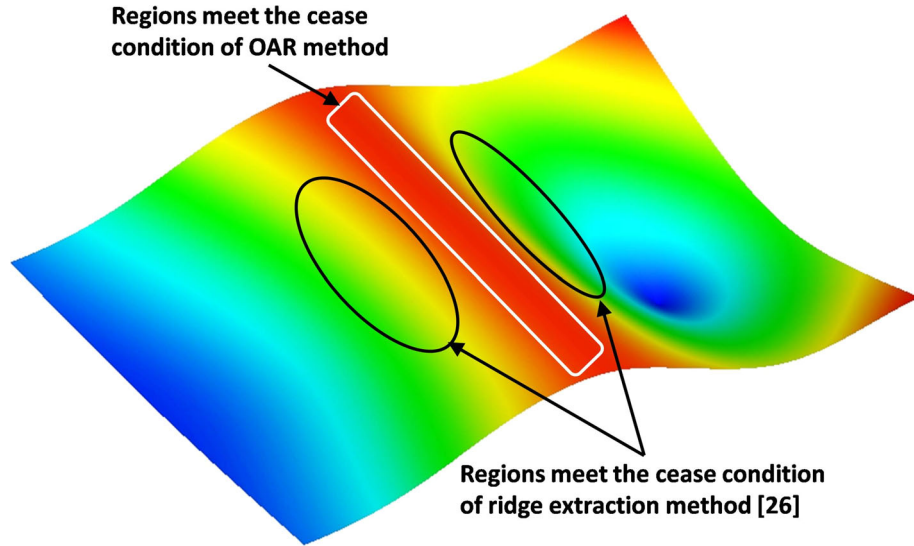


**Fig. 6** The explanation of the refinement region of ridge extraction method based on gradient ascending method (Mathur et al. 2007)

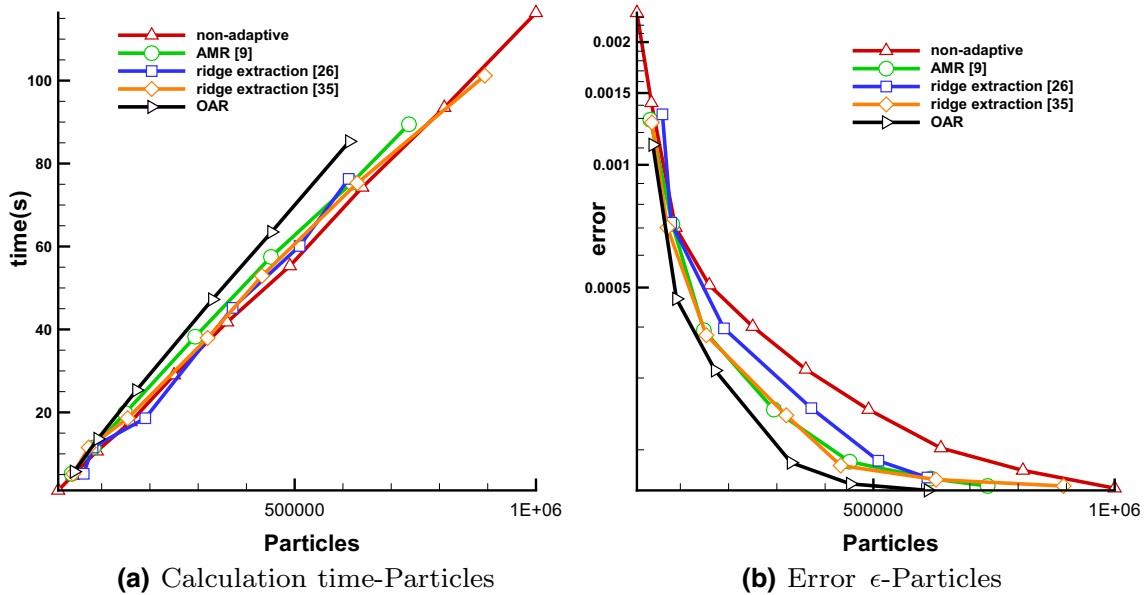


**Fig. 7** Comparison of the calculation time and errors of the non-adaptive and different adaptive criteria

In our calculation, the integration time is  $\Delta t = 1.78$  s. From the comparison of the different methods, we can find out that using adaptive methods would cut down the error in a huge amount and slightly add to the calculation time for a definitive total particle numbers. The ridge extraction method (Mathur et al. 2007) failed to find the correct refinement region because the regions that satisfy the cease criterion do not occur to be the region near the FTLE ridge, and would cause false positive problem in the calculation as shown in Fig. 6. It is because that in this case, the FTLE value near the ridge changes slowly relatively to other cases. The other ridge extraction method (Sadlo and Peikert 2007; Lipinski and Mohseni 2010), though could find FTLE ridge, refines so much area that the calculation burden is large. The proposed OAR method would spend slightly more calculation time as shown in Fig. 7a. However it successfully finds the correct refinement region, and thus cuts down the error faster than other methods as shown in Fig. 7b.

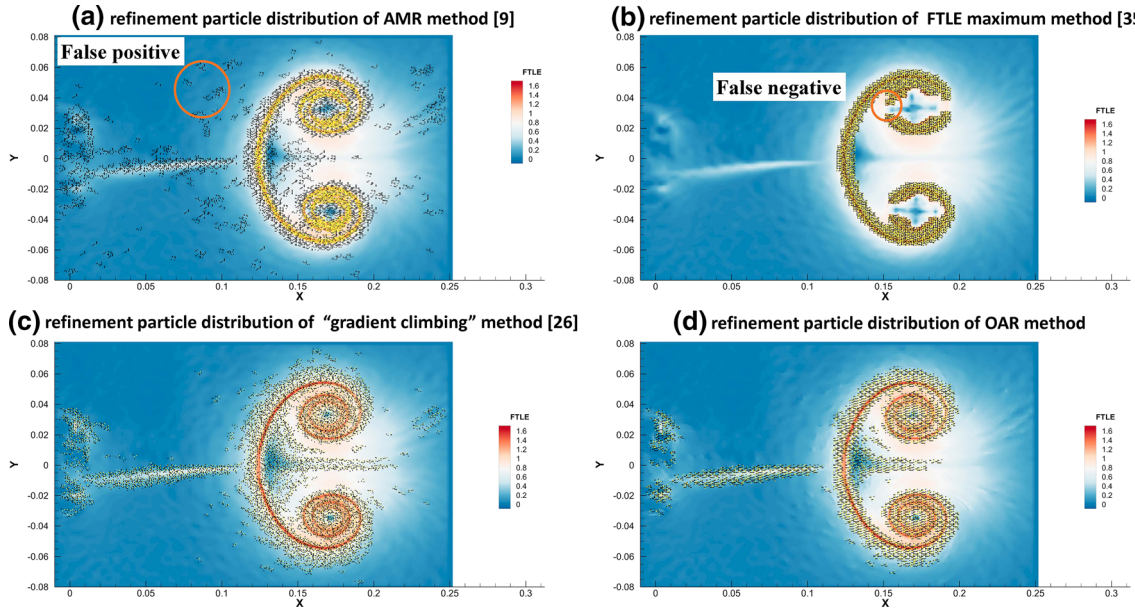


**Fig. 8** Single vortex ring. FTLE field and refinement particle distribution using an initial mesh of  $200 \times 100$  **a** AMR method (Garth et al. 2007) (total particle number is 340,931); **b** the proposed OAR method (total particle number is 381,713); **c** ridge extraction method based on the magnitude of FTLE (Sadlo and Peikert 2007; Lipinski and Mohseni 2010) (total particle number is 398,708); **d** ridge extraction method based on gradient ascending method (Mathur et al. 2007) (total particle number is 323,897)

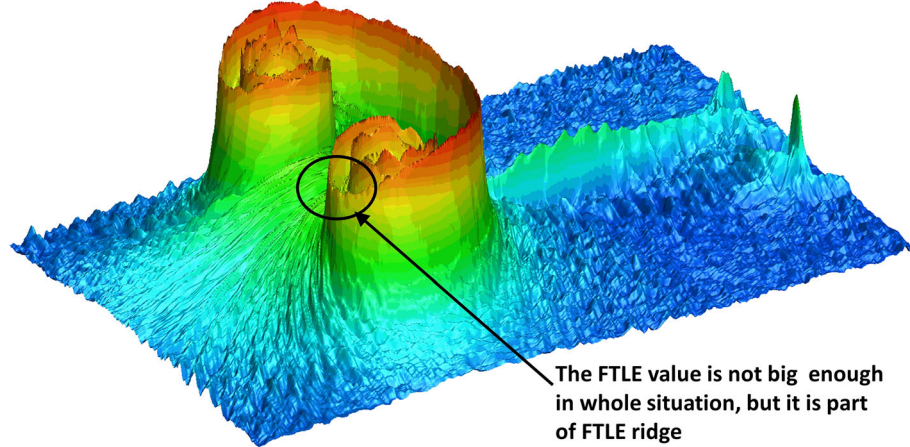


**Fig. 9** The explanation of the refinement region of ridge extraction method based on the magnitude of FTLE (Sadlo and Peikert 2007; Lipinski and Mohseni 2010)

#### 4.3 Experimental cases: single vortex

LCSs have long been used in the study of the generation, formation, evolution and pinch off of vortex rings (Shadden et al. 2006; O'Farrell and Dabiri 2010; Olcay and Krueger 2008). Especially in unsteady cases, LCS is superior to Euler methods in visualizing the details of vortex rings (Haller 2005).

The data we used in this article are a set of experimental data conducted by vortex ring generator. The experimental apparatus has been published by Qin et al. (2017, 2018).

Figure 8 shows vividly that the result of different refinement methods with initial coarse mesh (initial mesh of  $200 \times 100$ ). Figure 8a has false positive problem because of noise in initial data. From the comparison of the results, it can be found that the refinement of Fig. 8b is nearly wrong for it fails to capture some regions of FTLE ridge. The result also shows that this refinement criterion cannot be used in cases where the experimental error in the initial data can have an influence on the FTLE field. From Fig. 10b, the

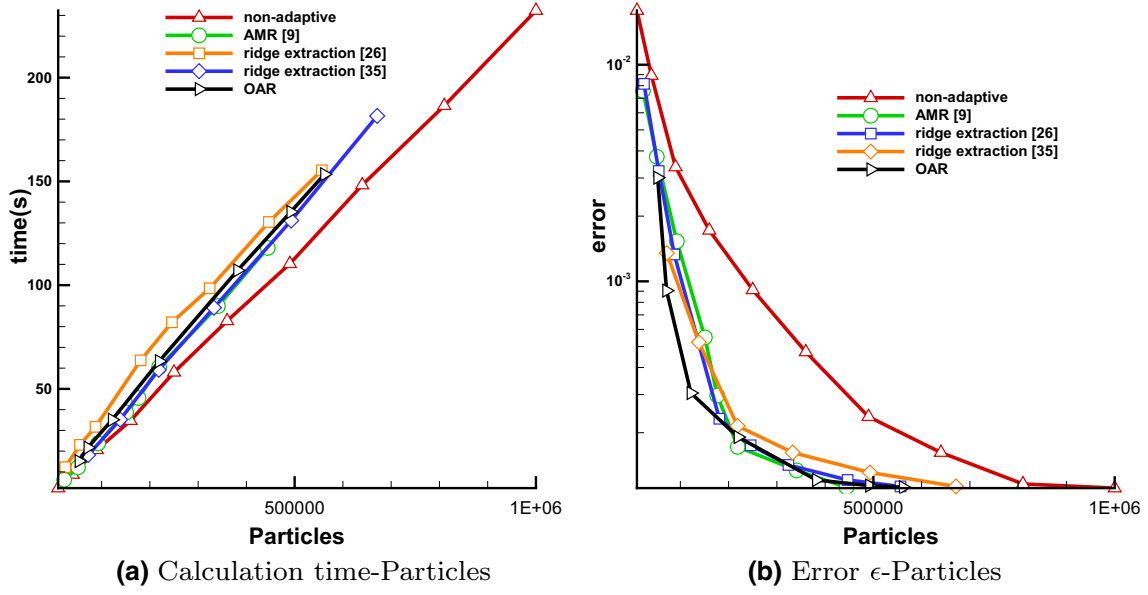


Fig. 10 Comparison of the calculation time and errors of the non-adaptive and different adaptive criteria

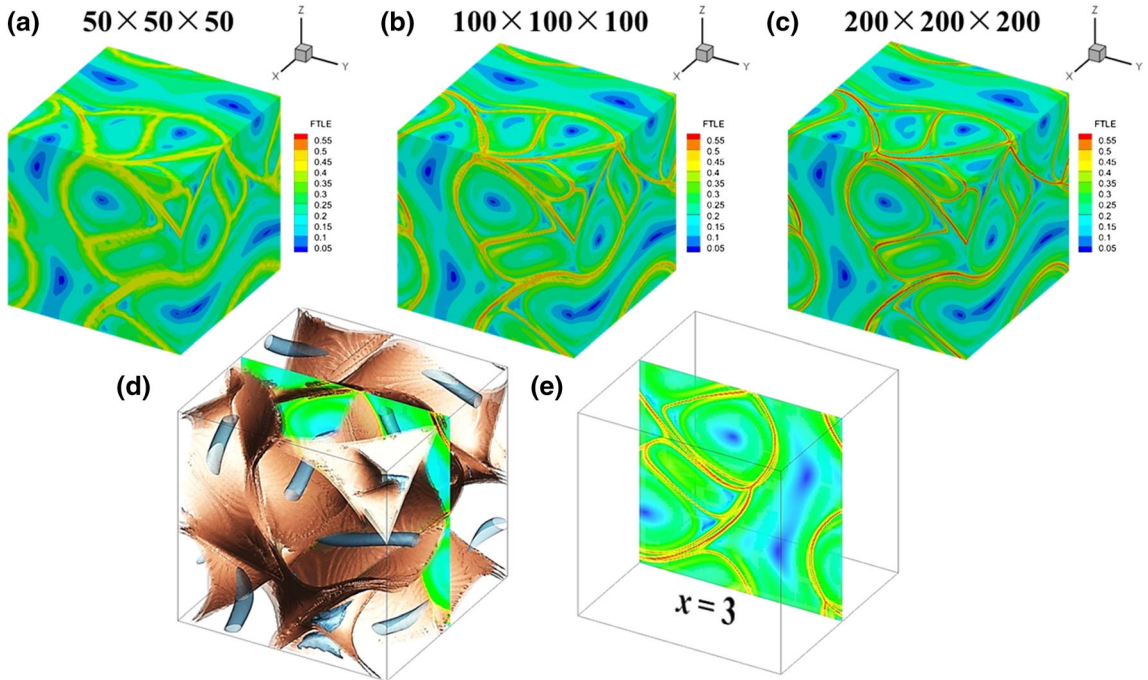
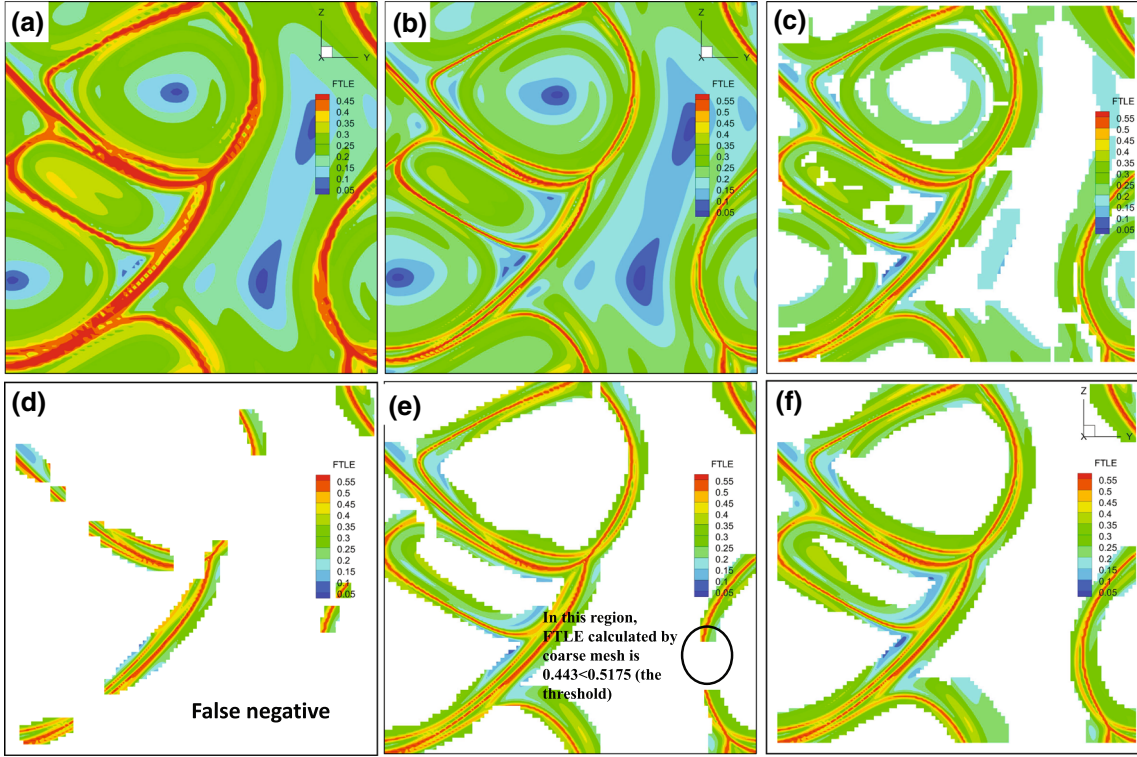


Fig. 11 The FTLE field of ABC flow: **a–c** shows the results calculated by different mesh scales; **d** shows the isosurface of  $\sigma_t^T(\mathbf{x}) = 0.4$  and  $\sigma_t^T(\mathbf{x}) = 0.1$ ; **e** shows the slice which is used to compare different methods in Fig. 12

reason is shown that the error in initial data would also bring error in FTLE field. However, these regions are not where we pay attention to. On the other hand, the FTLE isosurface is undulate, and thus FTLE value on parts of the FTLE ridge is not enough to be big when seeing from the whole viewpoint. Because of this, the method would give false negative result in the refinement and the result would perform bad in some certain regions as shown in Fig. 8b. Figure 8c shows similar result as the proposed OAR method except a small proportion of particles is dispersed in area with noise in initial data (Fig. 9).

Because of the difference in the refinement regions, the ability to reduce error for different methods is different as in Fig. 10. The proposed OAR method can reduce the error most quickly compared with other



**Fig. 12** ABC flow: FTLE field of  $x = 3$  section by **a** non-adaptive method using a mesh of  $100 \times 100 \times 100$ ; **b** non-adaptive method using a mesh of  $200 \times 200 \times 200$ ; **c** the proposed OAR method using an initial mesh of  $100 \times 100 \times 100$  (only show the refinement particles, total particle number is  $6.46 \times 10^6$ ); **d–f** ridge extraction method based on the magnitude of FTLE (Sadlo and Peikert 2007; Lipinski and Mohseni 2010) using an initial mesh of  $100 \times 100 \times 100$ ,  $\alpha$  equals to 0.95, 0.9, 0.7, respectively. (Only show the refinement particles, in which, the case of  $\alpha = 0.9$  is used in the comparison in Fig. 13.) The amounts of total particles are  $4.26 \times 10^6$ ,  $7.02 \times 10^6$ , and  $9.84 \times 10^6$

methods, and the ridge extraction method based on the magnitude of FTLE (Sadlo and Peikert 2007; Lipinski and Mohseni 2010) performs the worst. The larger the proportion of particles put near the FTLE ridge is, the faster the criterion can reduce error.

#### 4.4 Three-dimensional case: ABC flow

An example ABC flow is given, the speed field is as Eq. (18) (Sulman et al. 2013).

$$\begin{cases} u(\mathbf{x}) = A \sin z + C \cos y \\ v(\mathbf{x}) = B \sin x + A \cos z \\ w(\mathbf{x}) = C \sin y + B \cos x \end{cases} \quad (18)$$

The parameters and computational domain are  $A = 1, B = 0.8, C = 0.8, x, y, z \in [0, 2\pi]$ ,  $\Delta t = 1$  s. The calculated FTLE field is shown in Fig. 11. The resolution of mesh has the great effect on the visualization of LCS as shown in Fig. 11a–c. The mesh resolution is  $50 \times 50 \times 50$ ,  $100 \times 100 \times 100$  and  $200 \times 200 \times 200$ . Figure 11d shows the isosurface of the FTLE field. In order to compare the OAR method with AMR by magnitude of FTLE (Sadlo and Peikert 2007) (the parameter is chosen as  $\alpha = 0.9$ ), the slice of  $x = 3$  is compared in the following results as shown in Fig. 11e.

Detailed results comparison of  $x = 3$  between ridge extraction from magnitude of FTLE (Sadlo and Peikert 2007) and OAR is presented in Fig. 12. In OAR method, the final refinement region converges FTLE ridge as shown in Fig. 12c. It is clear that the proposed method can disperse refinement particles around the FTLE ridge. Because the parameter  $\alpha$  in extraction from magnitude of FTLE (Sadlo and Peikert 2007) is chosen subjectively, three cases are chosen to compare with the proposed method.  $\alpha$  is chosen to be 0.95, 0.9, 0.7 as shown in Fig. 12d–f. When  $\alpha$  is chosen to be 0.9, the amount of particle is near to the one of the

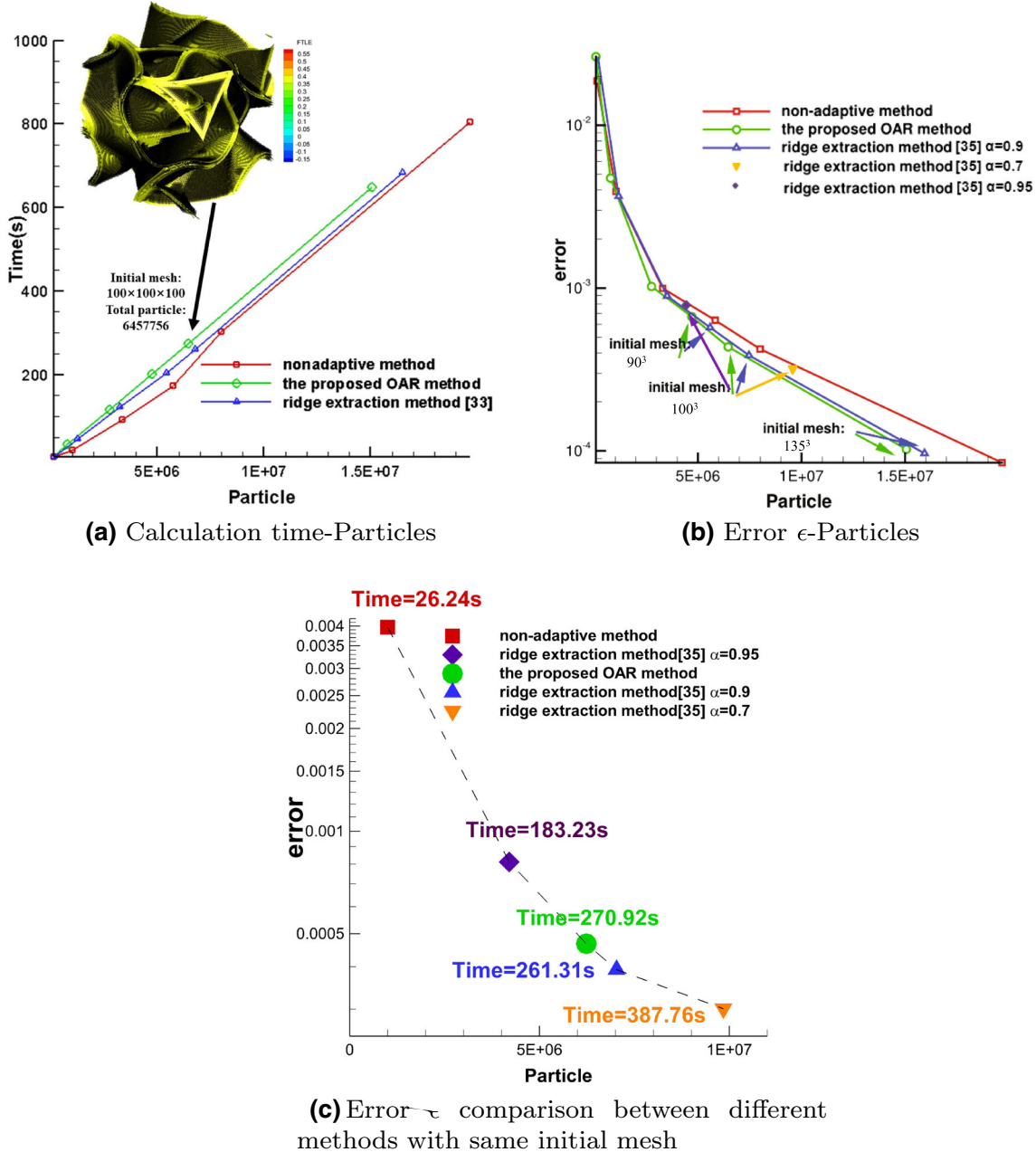


**Fig. 13** Comparison of the calculation time and errors of the non-adaptive and different adaptive criteria

proposed OAR method. In this case, Fig. 12e can show that due to the mean value of first layer 0.443 is lower than the threshold 0.5175, some certain region that needs to be refined is neglected. When  $\alpha$  is chosen to be 0.7, the ridge is refined, but as shown in Fig. 13, it would cost about 40% more time than the proposed method. When  $\alpha$  is chosen to be 0.95, only a small proportion of the ridge is refined and the calculation error is large. From the comparison, it can be found that the proposed method is prior to the method in Sadlo and Peikert (2007) not only because of its accuracy and efficiency, but also because of its objectivity in finding refinement regions. When applying the method in Sadlo and Peikert (2007), it may cost us a lot of time to choose a proper threshold. On the other hand, by using the proposed method, because it focuses only on the FTLE ridge, the refinement region is objective.

## 5 Conclusions

In this paper, we propose the application of objective-adaptive refinement (OAR) criterion based on modified ridge extraction method into finite-time Lyapunov exponent (FTLE) computation. Compared with the AMR method, the criterion has some advantages. The refinement rule can ensure that the correct position of refinement particles would be found. This character is especially important when the FTLE ridge is relatively mild or error is presented in the initial data. The efficiencies and accuracies of the proposed OAR with other adaptive refinement methods were compared by theoretical and experimental cases. Moreover, due to the characteristics of the method, the choice of the parameter is fully objective. Introducing the OAR criterion into LCS computation can cut down to number of refinement particles, and thus make the adaptive calculation of FTLE more efficient by a better extraction of FTLE ridge. For further development of this research, we may refer to some advanced adaptive method such as Barakat and Tricoche (2013) in order to reduce the number of refinement particles.

**Acknowledgements** The authors would like to thank the Center for High-Performance Computing of SJTU for providing the super computer  $\pi$  to support this research. This work is supported by the National Natural Science Foundation of China (NSFC-91741113) and National Science Foundation for Young Scientists of China (Grant No. 51676203). Furthermore, Geng Liang is appreciated in assistance in three-dimensional cases and refinement criterion. Also, Chunhui Tang, Haiyan Lin and Linying Li are appreciated in assisting the completion of the paper.

## References

- Barakat SS, Tricoche X (2013) Adaptive refinement of the flow map using sparse samples. *IEEE Trans Vis Comput Graph* 19(12):2753–2762
- Berger MJ, Colella PJ (1989) Local adaptive mesh refinement for shock hydrodynamics. *J Comput Phys* 82(1):64–84
- Beron Vera FJ, Olascoaga MJ, Haller G, Farazmand M, Trianes J, Wang Y (2015) Dissipative inertial transport patterns near coherent lagrangian eddies in the ocean. *Chaos* 25(8):087,412
- Blazevski D, Haller G (2014) Hyperbolic and elliptic transport barriers in three-dimensional unsteady flows. *Phys D Nonlinear Phenom* 273–274(2):46–62
- Chong MS, Perry AE, Cantwell BJ (1990) A general classification of three-dimensional flow fields. *Phys Fluids A* 2(5):765–777
- Duc LH, Siegmund S (2008) Hyperbolicity and invariant manifolds for planar nonautonomous systems on finite time intervals. *Int J Bifurc Chaos* 18(03):0802,056
- Fortin A, Briffard T, Garon A, Briffard T, Garon A (2015) A more efficient anisotropic mesh adaptation for the computation of lagrangian coherent structures. *J Comput Phys* 285(C):100–110
- Froyland G, Padberg-Gehle K (2014) Almost-invariant and finite-time coherent sets: directionality, duration, and diffusion. Springer, New York, pp 171–216
- Garth C, Gerhardt F, Tricoche X, Hagen H (2007) Efficient computation and visualization of coherent structures in fluid flow applications. *IEEE Trans Vis Comput Graph* 13(6):1464–1471
- Green MA, Rowley CW, Haller G (2007) Detection of lagrangian coherent structures in three-dimensional turbulence. *J Fluid Mech* 572(572):111–120
- Hadjighasem A, Haller G (2014) Geodesic transport barriers in jupiter's atmosphere: a video-based analysis. *IEEE Trans Commun* 58(1):536–551
- Haller G (2001) Distinguished material surfaces and coherent structures in three-dimensional fluid flows. *Phys D Nonlinear Phenom* 149(4):248–277
- Haller G (2005) An objective definition of a vortex. *J Fluid Mech* 525(525):1–26
- Haller G (2011) A variational theory of hyperbolic lagrangian coherent structures. *Phys D Nonlinear Phenom* 240(7):574–598
- Haller G (2015) Lagrangian coherent structures. *Annu Rev Fluid Mech* 47(1):137–162
- Haller G, Yuan G (2000) Lagrangian coherent structures and mixing in two-dimensional turbulence. *Phys D Nonlinear Phenom* 147(3C4):352–370
- Huang W, Russell RD (2011) Adaptive moving mesh methods. Springer, New York
- Hunt JCR (1988) Eddies, streams, convergence zones in turbulent flows. In: Studying turbulence using numerical simulation databases, pp 193–208
- Jeong J, Hussain F (1995) On the identification of a vortex. *J Fluid Mech* 285(285):69–94
- Jimbo T, Tanahashi T (2003) Numerical simulations of unsteady shock waves around complex bodies. *J Vis* 6(3):212–212
- Karch GK, Sadlo F, Weiskopf D, Ertl T (2016) Visualization of 2d unsteady flow using streamline-based concepts in space-time. *J Vis* 19(1):115–128
- Karrasch D, Huhn F, Haller G (2015) Automated detection of coherent lagrangian vortices in two-dimensional unsteady flows. *Proc R Soc A Math Phys Eng Sci* 471(2173):20140639
- Keith W, Demetri T (1991) Modeling and animating faces using scanned data. *J Vis Comput Anim* 2(4):123–128
- Liang G, Yu B, Zhang B, Xu H, Liu H (2019) Hidden flow structures in compressible mixing layer and a quantitative analysis of entrainment based on lagrangian method. *J Hydrom*. <https://doi.org/10.1007/s42241-019-0027-z>
- Lipinski D, Mohseni K (2010) A ridge tracking algorithm and error estimate for efficient computation of lagrangian coherent structures. *Chaos* 20(1):017,504

- Mathur M, Haller G, Peacock T, Ruppert-Felsot JE, Swinney HL (2007) Uncovering the lagrangian skeleton of turbulence. *Phys Rev Lett* 98(14):144,502
- Miron P, Vtel J, Garon A, Delfour M, Hassan ME (2012) Anisotropic mesh adaptation on lagrangian coherent structures. *J Comput Phys* 231(19):6419–6437
- Ng KW, Wong YP (2007) Adaptive model simplification in real-time rendering for visualization. *J Vis* 10(1):111–121
- O'Farrell C, Dabiri JO (2010) A lagrangian approach to identifying vortex pinch-off. *Chaos* 20(1):261–300
- Olcay AB, Krueger PS (2008) Measurement of ambient fluid entrainment during laminar vortex ring formation. *Exp Fluids* 44(2):235–247
- Onu K, Huhn F, Haller G (2014) Lcs tool: a computational platform for lagrangian coherent structures. *J Comput Sci* 7:26–36
- Plewa T, Linde T, Weirs VG, Numerik (2005) Adaptive mesh refinement—theory and applications. Springer, Berlin
- Qin S, Liu H, Xiang Y (2017) Lagrangian flow visualization of multiple co-axial co-rotating vortex rings. *J Vis* 31:1–9
- Qin S, Liu H, Xiang Y (2018) On the formation modes in vortex interaction for multiple co-axial co-rotating vortex rings. *Phys Fluids* 30(1):011,901
- Sadlo F, Peikert R (2007) Efficient visualization of lagrangian coherent structures by filtered amr ridge extraction. *IEEE Trans Vis Comput Graph* 13(13):1456–1463
- Shadden SC, Dabiri JO, Marsden JE (2006) Lagrangian analysis of fluid transport in empirical vortex ring flows. *Phys Fluids* 18(4):047,105
- Shadden SC, Katija K, Rosenfeld M, Marsden JE, Dabiri JO (2007) Transport and stirring induced by vortex formation. *J Fluid Mech* 593(593):315–331
- Sulman MHM, Huntley HS, Lipphardt BL Jr, Kirwan AD Jr (2013) Leaving flatland: diagnostics for lagrangian coherent structures in three-dimensional flows. *Phys D Nonlinear Phenom* 258(5):77–92
- Tallapragada P, Ross SD, Schmale III DG (2011) Lagrangian coherent structures are associated with fluctuations in airborne microbial populations. *Chaos* 21(3):033,122
- Tang W, Chan PW, Haller G (2010) Accurate extraction of lagrangian coherent structures over finite domains with application to flight data analysis over hong kong international airport. *Chaos* 20(1):017,502
- Tian S, Gao Y, Dong X, Liu C (2018) Definitions of vortex vector and vortex. *J Fluid Mech* 849:312C339. <https://doi.org/10.1017/fm.2018.406>
- Wang H, Ai Z, Cao Y, Xiao L (2016) A parallel preintegration volume rendering algorithm based on adaptive sampling. *J Vis* 19(3):437–446
- Zhang Y, Liu K, Xian H, Du X (2017) A review of methods for vortex identification in hydroturbines. *Renew Sustain Energy Rev* 81:1269–1285

**Publisher's Note** Springer Nature remains neutral with regard to jurisdictional claims in published maps and institutional affiliations.